Intrinsic lattice thermal conductivity of Si/Ge and GaAs/AlAs superlattices

A. Ward and D. A. Broido
Department of Physics, Boston College, Chestnut Hill, Massachusetts 02467, USA
(Received 29 February 2008; revised manuscript received 29 April 2008; published 30 June 2008)

We present a theory of the intrinsic lattice thermal conductivity in Si/Ge-based and GaAs/AlAs quantum well superlattices using an exact iterative solution of the inelastic phonon Boltzmann equation. An adiabatic bond charge model is employed to accurately represent the phonon dispersions and the empirical anharmonic force constants are introduced yielding the measured values for bulk thermal conductivities. We show that the kinematic constraints of the superlattice decrease the phonon-phonon scattering, resulting in higher intrinsic lattice thermal conductivities than those calculated from constant relaxation-time approximations and simple model phonon dispersions. The role of mini-umklapp processes, produced as a result of zone-folding in superlattices, is also addressed. Finally, we find larger calculated intrinsic lattice thermal conductivities of GaAs/AlAs superlattices than those predicted from a relaxation-time approach, implying that interface scattering plays a more important role than previously documented. These findings are consistent with experimental measurements for short-period GaAs/AlAs structures.

DOI: 10.1103/PhysRevB.77.245328 PACS number(s): 63.22.−m, 63.20.kg, 66.70.−f

I. INTRODUCTION

The thermal transport properties of semiconductor nanostructures have attracted considerable interest in recent years.[1] This is due in part to the changes in the measured lattice thermal conductivity in these structures compared to their bulk constituents,[2–7] which makes them potentially useful materials for thermoelectrics,[8,9] and other applications involving microelectronic devices and circuits.[1] A dramatic example of this phenomenon occurs in quantum well superlattices (SLs), where order-of-magnitude decreases have been observed in the thermal conductivity along the growth axis of Si/Ge,[2] GaAs/AlAs,[3,4] and Bi_2Te_3/Sb_2Te_3 structures.[5]

The significant drop in the lattice thermal conductivity in SLs, κ_{SL}, results primarily from two mechanisms. The first involves phonon scattering by imperfections at the SL interfaces.[10] This *extrinsic* mechanism depends on sample quality: a greater roughness at each interface leads to a greater number of scattered phonons and a lowering of κ_{SL}. The second mechanism is *intrinsic*. To understand it, we first look at the bulk material.

Above a few tens of degrees Kelvin, the lattice thermal conductivity of high quality bulk semiconductors is determined primarily by phonon-phonon scattering, which arises due to the anharmonicity of the interatomic potential.[11,12] Unlike phonon scattering by defects, impurities, or boundaries, anharmonic phonon-phonon scattering is an intrinsic resistive process that limits the maximum achievable lattice thermal conductivity at each temperature. In a SL structure, the intrinsic part of the thermal conductivity, $\kappa_{SL}^{(i)}$, is changed compared to its bulk counterpart because of the periodic variation of the two constituent atoms. This variation modifies the phonon dispersions. One consequence of this is that the average group velocity of the acoustic modes is reduced, thereby acting to lower $\kappa_{SL}^{(i)}$. Calculations based on the constant relaxation-time approximation (CRTA) and simple model lattice dynamics have predicted order-of-magnitude reductions in $\kappa_{SL}^{(i)}$ for Si/Ge structures based on this effect.[13,14] Another consequence was highlighted in recent calculations of $\kappa_{SL}^{(i)}$ for Si/Ge-based SLs.[15] This work implemented an exact solution of the phonon Boltzmann equation to show that the kinematic constraints of energy and momentum conservation for three-phonon scattering become more restrictive in SLs, and this acts to raise $\kappa_{SL}^{(i)}$. A competition between these two effects exists, which varies with the masses of the constituent materials and the period of the SL.

The calculations in Ref. 15 used a Keating model[16] to describe the harmonic and anharmonic interatomic forces. The Keating model does not accurately describe the flat transverse-acoustic phonon branches that characterize most diamond and zinc-blende semiconductors, which are the constituent materials of many SLs. Since the kinematic constraints are completely determined by the phonon dispersions [see Eq. (1)], it is of interest to calculate $\kappa_{SL}^{(i)}$ using accurate descriptions of the SL phonon dispersions.

In this paper, we develop a theoretical approach to calculate the intrinsic lattice thermal conductivity of SLs. This approach combines an exact solution of the inelastic phonon Boltzmann equation with accurate descriptions of the phonon dispersions obtained from an adiabatic bond charge model.[17,18] We use this model to assess how $\kappa_{SL}^{(i)}$ depends on accurate representations of the phonon dispersion as well as the mass ratio of the constituent atoms. In addition, we investigate the significance of the additional three-phonon umklapp processes ("mini-umklapp" processes) that were proposed to occur in SLs by Ren and Dow.[19] Finally, we also calculate $\kappa_{SL}^{(i)}$ as a function of temperature for short-period GaAs/AlAs SLs and compare our results with measured values. This procedure allows us to indirectly evaluate the extrinsic contribution to the lattice thermal conductivity, $\kappa_{SL}^{(e)}$.

We focus on the temperature range around room temperature where three-phonon scattering is the dominant scattering process. In Sec. II, we develop the theory of the intrinsic lattice thermal conductivity of SLs. Section III describes the adiabatic bond charge model used to calculate the SL phonon dispersions and the central potential model used to represent the anharmonic interatomic forces. In Sec. IV the calculated

intrinsic lattice thermal conductivities of Si/Ge-based and GaAs/AlAs SLs are presented and discussed. Section V gives a summary and conclusions.

II. THEORY OF INTRINSIC LATTICE THERMAL CONDUCTIVITY

We develop here a Boltzmann transport theory for the intrinsic lattice thermal conductivity of a perfect, defect-free SL, $\kappa_{\mathrm{SL}}^{(i)}$. Around room temperature, the vibrating lattice atoms sample the anharmonicity of the interatomic potential causing phonons to scatter from one another and producing intrinsic thermal resistance. The most significant processes involve three phonons.[11,12] These processes are constrained to satisfy conservation of energy and quasimomentum,[11,12]

$$\omega_j(\mathbf{q}) \pm \omega_{j'}(\mathbf{q}') = \omega_{j''}(\mathbf{q}''), \quad \mathbf{q} \pm \mathbf{q}' = \mathbf{q}'' + \mathbf{K}, \tag{1}$$

where j is the SL phonon branch index, $\mathbf{q}$ is the phonon wave vector, $\omega_j(\mathbf{q})$ is the phonon frequency, and $\mathbf{K}$ is a reciprocal-lattice vector that is zero for normal processes and nonzero for umklapp processes. We refer to Eq. (1) as the kinematic constraints, which restrict the phase space of phonons that can participate in scattering events.

A small temperature gradient, ∇T, is taken to perturb the phonon distribution function $n_\lambda = n_{0\lambda} + n_{1\lambda}$, where λ is a short-hand for $(\mathbf{q},j)$, $n_{0\lambda} \equiv n_0(\omega_\lambda)$ is the equilibrium (Bose) phonon distribution function, and the nonequilibrium part, $n_{1\lambda}$, produces the thermal current. The linearized phonon Boltzmann equation is[11,12]

$$\mathbf{v}_\lambda \cdot \nabla T \frac{\partial n_{0\lambda}}{\partial T} = \sum_{\lambda'\lambda''} \left[W^{+}_{\lambda\lambda'\lambda''}(\Psi_{\lambda''} - \Psi_{\lambda'} - \Psi_\lambda) + \frac{1}{2} W^{-}_{\lambda\lambda'\lambda''}(\Psi_{\lambda''} + \Psi_{\lambda'} - \Psi_\lambda) \right], \tag{2}$$

where $\mathbf{v}_\lambda$ is the phonon velocity in mode λ, and $\Psi_\lambda = n_{1\lambda}/[n_{0\lambda}(n_{0\lambda}+1)]$. The presence of $\Psi_{\lambda'}$ and $\Psi_{\lambda''}$ conveys the inelastic nature of the phonon-phonon scattering. Replacement of the right-hand side of Eq. (2) by $-n_{1\lambda}/\tau$, where τ is an adjustable constant scattering time, gives the commonly used CRTA.[11–14] The sums on the right-hand side of Eq. (2) are over the phase space of allowed three-phonon processes determined by the kinematic constraints [Eq. (1)].

The three-phonon-scattering rates, $W^{\pm}_{\lambda\lambda'\lambda''}$, determined from Fermi's golden rule, are

$$W^{\pm}_{\lambda\lambda'\lambda''} = \frac{\hbar\pi}{4N} \frac{(n_{0\lambda}+1)(n_{0\lambda'}+1/2 \pm 1/2)n_{0\lambda''}}{\omega_\lambda \omega_{\lambda'} \omega_{\lambda''}} \times |\Phi_{\pm}(\lambda,\lambda',\lambda'')|^2 \delta(\omega_\lambda \pm \omega_{\lambda'} - \omega_{\lambda''}). \tag{3}$$

Here, N is the number of SL unit cells and the delta function ensures energy conservation. The phonon frequencies, $\{\omega_\lambda\}$, are determined by diagonalizing the dynamical matrix, whose construction will be discussed in the next section. The three-phonon-scattering matrix elements, $\Phi_{\pm}(\lambda,\lambda',\lambda'')$, which measure the strength of each scattering event, are

$$\Phi(j,\mathbf{q};j',\mathbf{q}';j'',\mathbf{q}'') = \sum_{\kappa} \sum_{\ell'\kappa'} \sum_{\ell''\kappa''} \sum_{\alpha\beta\gamma} \Phi_{\alpha\beta\gamma}(0\kappa,\ell'\kappa',\ell''\kappa'') \times e^{i\mathbf{q}'\cdot\mathbf{R}_{\ell'}} e^{i\mathbf{q}''\cdot\mathbf{R}_{\ell''}} \frac{e^{j}_{\alpha\kappa}(\mathbf{q}) e^{j'}_{\beta\kappa'}(\mathbf{q}') e^{j''}_{\gamma\kappa''}(\mathbf{q}'')}{\sqrt{M_\kappa M_{\kappa'} M_{\kappa''}}}. \tag{4}$$

Here, $\mathbf{R}_\ell$ is a lattice vector in the ℓth SL unit cell, κ specifies an atom in this cell whose mass is M_κ, and α, β, and γ are Cartesian components. $\Phi_{\alpha\beta\gamma}(0\kappa,\ell'\kappa',\ell''\kappa'')$ is the third order anharmonic force constant for the indicated triplet of atoms, and the es are phonon eigenvectors.

We have solved exactly the phonon Boltzmann equation [Eq. (2)] for the nonequilibrium distribution functions $\{\Psi_\lambda\}$ employing an iterative approach, which is described in detail in Refs. 20–23. These are used to calculate the phonon thermal-conductivity tensor, $\kappa_{\alpha\beta}$, which relates an applied temperature gradient in the β direction to the resulting heat current per unit area in the α direction through Fourier's law: $J_\alpha = -\Sigma_\beta \kappa_{\alpha\beta} \partial T/\partial x_\beta$. Here, $\kappa_{\alpha\beta}$ can be expressed as

$$\kappa_{\alpha\beta} = \sum_\lambda C_\lambda v_{\lambda\alpha} v_{\lambda\beta} \tau_{\lambda\beta}, \tag{5}$$

where $C_\lambda = k_B(\hbar\omega_\lambda/k_BT)^2 n_{0\lambda}(n_{0\lambda}+1)$ is the contribution per mode $(\mathbf{q},j)$ to the specific heat and the scattering times, $\tau_{\lambda\beta}$, are directly related to Ψ_λ.[20–23]

The only inputs to this Boltzmann transport approach are the harmonic and anharmonic interatomic force constants (IFCs). The harmonic IFCs are needed to calculate the phonon frequencies and eigenvectors while the anharmonic IFCs are required for the evaluation of the three-phonon matrix elements in Eq. (4). Determination of these IFCs is discussed in the next section.

III. HARMONIC AND ANHARMONIC INTERATOMIC FORCE CONSTANTS FOR SLs

We use an adiabatic bond charge (ABC) model[17,18] to calculate the SL phonon dispersions. The ABC model has been shown to provide excellent fits to experimental dispersion curves for a large number of semiconductors using a small number of fit parameters (four for diamond structure and six for zinc-blende structure). In the ABC model, point bond charges (bc), placed between each pair of ions, move adiabatically to model the bonding electrons. There are four main interactions: (a) the central potential interaction between each ion and its four nearest-neighbor ions (ion-ion), (b) the central potential interaction between each ion and its four nearest-neighbor bond charges (ion-bc), (c) the bond-bending interaction between pairs of bond charges and their shared ion (bc-bc), and (d) the Coulomb interaction between all ions, between ions and bond charges, and between all bond charges. The first three interactions are short-range; the last is long-range. In zinc-blende materials, for (b) cation-bc and anion-bc interactions are taken to be distinct, as are (c) bc-cation-bc and bc-anion-bc interactions. Also, a direct central potential interaction is included between bond charges.[18]

We consider a SL based on a diamond structure and lattice constant, α. The SL axis is oriented along the [001] direction.

A coordinate system is chosen with x and y axes along [110] and $[\bar{1}10]$ directions (rotated by 45° from the cubic [100] and [010] directions), and z axis along [001]. In this coordinate system, the atoms in each plane perpendicular to the [001] direction reside on square lattices of side $h_1=a/\sqrt{2}$ and the x-y coordinates of the atoms repeat every four planes along the [001] direction. We consider SL unit cells containing $2N$ atoms and $4N$ bond charges, with N being even. Thus, the unit cell for a 2×2 Si/Ge [001] SL contains silicon atoms at locations, (0,0,0) and $(h_1/2,0,a/4)$ followed by germanium atoms at $(h_1/2,-h_1/2,a/2)$ and $(0,-h_1/2,3a/4)$ with the eight bond charges placed midway between pairs of atoms. The SL unit cell is rectangular with dimension $h_1\times h_1\times a$, twice the size of an fcc unit cell. The corresponding first Brillouin zone is also rectangular with dimension $2\pi/h_1\times2\pi/h_1\times2\pi/a$.

The SL dynamical matrix has size $18N\times18N$ and can be written as[17]

$$D_{\alpha\beta}(\kappa\kappa',\mathbf{q})=D_{\alpha\beta}^{(SR)}(\kappa\kappa',\mathbf{q})+D_{\alpha\beta}^{(C)}(\kappa\kappa',\mathbf{q}), \tag{6}$$

where the short-range (SR) part is

$$D_{\alpha\beta}^{(SR)}(\kappa\kappa',\mathbf{q})=\sum_{\ell'}\Phi_{\alpha\beta}^{(SR)}(0\kappa,\ell'\kappa')\times\exp\{-i\mathbf{q}\cdot[\mathbf{x}(0\kappa)-\mathbf{x}(\ell'\kappa')]\}, \tag{7}$$

and $\Phi_{\alpha\beta}^{(SR)}(0\kappa,\ell'\kappa')$ contains the combination of harmonic IFCs defined in (a), (b), and (c) above. The Coulombic part of the dynamical matrix, $D_{\alpha\beta}^{(C)}(\kappa\kappa',\mathbf{q})$, is evaluated using the Ewald transformation.[24] A brief discussion of these IFCs is included in the Appendix. More detailed descriptions of the ABC model can be found in Refs. 17 and 18.

In the ABC model, the bond charge masses are taken to vanish, leading to a renormalized dynamical matrix for the ions,

$$D^{(\mathrm{ren})}=D^{(\mathrm{ion\text{-}ion})}-D^{(\mathrm{ion\text{-}bc})\dagger}[D^{(\mathrm{bc\text{-}bc})}]^{-1}D^{(\mathrm{ion\text{-}bc})}, \tag{8}$$

where the Ds are the ion-ion, ion-bc, and bc-bc parts of the dynamical matrix in Eq. (6). The phonon frequencies $\omega_j(\mathbf{q})$ and eigenvectors $\hat{e}_j(\mathbf{q})$ are determined by diagonalizing the $6N\times6N$ eigenvalue equation,

$$\sum_{\kappa',\beta}\frac{1}{\sqrt{M_\kappa M_{\kappa'}}}D_{\alpha\beta}^{(\mathrm{ren})}(\kappa\kappa',\mathbf{q})e_{\beta\kappa'}(\mathbf{q})=\omega^2(\mathbf{q})e_{\alpha\kappa}(\mathbf{q}). \tag{9}$$

For the anharmonic IFCs appearing in Eq. (4), we take only nearest-neighbor central potential third-order anharmonic interactions between ions. This introduces only one additional parameter, $\phi'''_{\mathrm{ion\text{-}ion}}$, which appears in Eq. (A6). The anharmonic IFCs are chosen by requiring that the calculated room-temperature lattice thermal conductivity for the bulk material of either constituent of the SL must match the corresponding measured lattice thermal conductivity. We choose for $\phi'''_{\mathrm{ion\text{-}ion}}$ the values −43.8, −36.0, and −29.6 for Si, Ge, and GaAs in units of eV/Å^3. This gives calculated room-temperature lattice thermal conductivities of 160.4, 68.9, and 45.9 W/m-K, respectively, in good agreement with the corresponding measured values in Refs. 25–27. For AlAs, the thermal conductivity is not well characterized so we take $\phi'''_{\mathrm{ion\text{-}ion}}$ to be the same as that for GaAs.

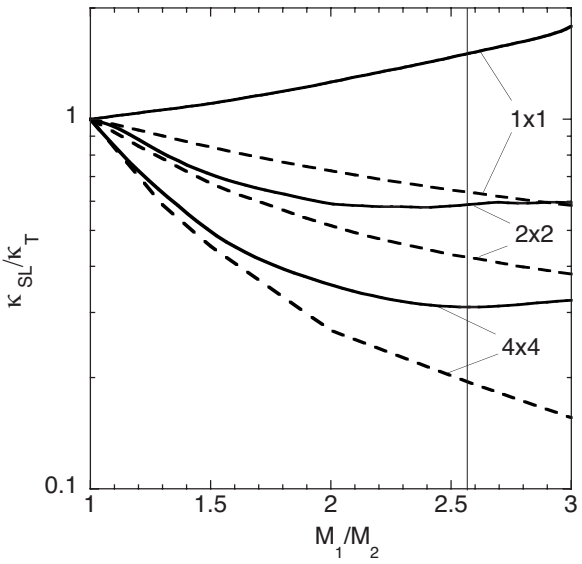

FIG. 1. Calculated intrinsic lattice thermal conductivity $\kappa_{\mathrm{SL}}^{(i)}$ of 1×1, 2×2, and 4×4 Si/Ge-based SLs as a function of the mass ratio of constituent atoms, M_1/M_2. The dashed lines are for the CRTA while the solid lines are obtained from the full calculation. The thin vertical line indicates the Ge/Si mass ratio.

IV. RESULTS AND DISCUSSION

We first consider the calculated lattice thermal conductivity of Si/Ge-based short-period SLs. All results are scaled with reference to a hypothetical template material whose harmonic and anharmonic IFCs, as well as the atomic masses, are taken to be the geometric averages of those for bulk Si and Ge: $M_t=\sqrt{M_{\mathrm{Si}}M_{\mathrm{Ge}}}$ with $M_{\mathrm{Ge}}=72.64$ and $M_{\mathrm{Si}}=28.09$. The SL is then generated by modifying the constituent atomic masses, M_1 and M_2, along the [001] SL axis. These masses are chosen so that M_1 (M_2) increases to fM_t (decreases to M_t/f) with $f>1$, in such a way that their geometric mean remains equal to the template mass: $\sqrt{M_1M_2}=M_t$.

We first investigate the dependence of $\kappa_{\mathrm{SL}}^{(i)}$ of Si/Ge-based short-period SLs on the mass ratio of the constituent atoms, M_1/M_2. Figure 1 displays the calculated $\kappa_{\mathrm{SL}}^{(i)}$, scaled by that of the template material, $\kappa_t^{(i)}$, as a function of M_1/M_2, for 1×1, 2×2, and 4×4 period SLs. The dashed lines show the results for the CRTA while the solid lines are those obtained from the full iterative approach. For the CRTA, $\kappa_{\mathrm{SL}}^{(i)}$ decreases with increasing mass ratio for all SL periods. As M_1/M_2 increases, the heat-carrying acoustic branches become flatter, which results in a lowering of the average group velocity and frequencies in these branches, and a consequent lowering of $\kappa_{\mathrm{SL}}^{(i)}$. This effect becomes more pronounced with increasing SL periods. The thin vertical line highlights this behavior for the Si/Ge SL (where $M_1=M_{\mathrm{Ge}}$ and $M_2=M_{\mathrm{Si}}$).

The full calculations (solid lines) exhibit more modest decreases in $\kappa_{\mathrm{SL}}^{(i)}$ than the CRTA. This behavior reflects the decrease in the phase space for three-phonon scattering that

TABLE I. Comparison of the calculated $\kappa_{\mathrm{SL}}^{(i)}/\kappa_t^{(i)}$ from the CRTA and full approach for 1×1, 2×2, 4×4, and 8×8 Si/Ge SLs.

	1×1	2×2	4×4	8×8
CRTA	0.63	0.42	0.19	0.14
Full solution	1.42	0.59	0.30	0.20

occurs for increasing M_1/M_2. The three-phonon phase space is dictated by the kinematic constraints in Eq. (1). The flattening of the acoustic branches that occurs with increasing M_1/M_2 makes these constraints more difficult to satisfy. The corresponding reduction in the three-phonon-scattering rates produces increased scattering times, $\tau_{\lambda\alpha}$, in Eq. (5) and hence larger $\kappa_{\mathrm{SL}}^{(i)}$ compared to the CRTA case. It is interesting that $\kappa_{\mathrm{SL}}^{(i)}/\kappa_t^{(i)}$ for the 2×2 and 4×4 SLs saturate for large mass ratios at values significantly larger than the order-of-magnitude reductions in $\kappa_{\mathrm{SL}}^{(i)}$, which have been predicted to occur from calculations based on the CRTA and simple models for the phonon dispersions.[13,14]

For the 1×1 SL the effect of the phase-space reduction is strong enough to raise $\kappa_{\mathrm{SL}}^{(i)}$ above the template value. This can be understood as follows. The 1×1 SL along the [001] direction is, in fact, just a zinc-blende structure with Si and Ge being the basis atoms. It has been pointed out previously[15] that three-phonon scattering in zinc-blende materials is reduced with increasing M_1/M_2 because of the increased gap between acoustic and optic modes that freezes out triplet scattering channels involving acoustic-optic phonon combinations.[28] This reduced scattering causes the observed increase in $\kappa_{\mathrm{SL}}^{(i)}$ above the template value for the 1×1 SL.

Table I lists the ratio $\kappa_{\mathrm{SL}}^{(i)}/\kappa_t^{(i)}$ for the Si/Ge case ($M_1=M_{\mathrm{Ge}}$ and $M_2=M_{\mathrm{Si}}$) for different $N\times N$ SLs using both the CRTA (first row) and full iterative (second row) calculations. Note the higher values of $\kappa_{\mathrm{SL}}^{(i)}/\kappa_t^{(i)}$ for the full solution over the CRTA for all cases. Also, the magnitude of the reduction in $\kappa_{\mathrm{SL}}^{(i)}/\kappa_t^{(i)}$ decreases with increasing SL period, suggestive of the formation of a minimum, as has been observed experimentally.[29] CPU time and memory constraints have precluded our consideration of larger period SLs to verify this behavior.

To further illustrate the interplay between the flattening of the SL dispersions and the three-phonon scattering that occurs with increasing M_1/M_2, we plot in Fig. 2 the log of the square of the three-phonon matrix elements, $|\Phi|^2$, for a 4×4 Si/Ge-based SL versus the number of energy and momentum-conserving scattering events obtained from our three-phonon phase-space search algorithm for a typical density of $\mathbf{q}$ points in the SL Brillouin zone. The solid line is for the template case, $M_1=M_2=M_t$, the crosses are for a slightly larger value, $M_1/M_2=1.001$, the dotted line is for $M_1/M_2=1.1$, and the open squares are for the Si/Ge case $M_1/M_2=2.58$. Consider first the template case, which exhibits a clearly separated two-peak structure. The smaller right peak corresponds to events that provide a contribution to the three-phonon-scattering rates in Eq. (3), whereas the large left peak corresponds to the mini-umklapp processes that are unique to the SL.[19] These mini-umklapp events are many

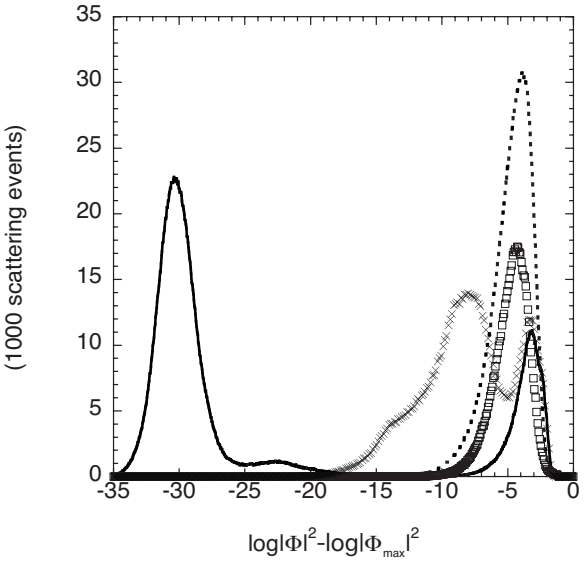

FIG. 2. The log of the square of the three-phonon matrix elements, $|\Phi|^2$, scaled by the maximum value found for all events, $|\Phi_{\mathrm{max}}|^2$, for a 4×4 Si/Ge-based SL versus the number of energy and momentum-conserving scattering events. The solid line is for $M_1=M_2$, the crosses are for $M_1=1.001M_2$, the dotted line is for $M_1=1.1M_2$, and open squares are for $M_1=M_{\mathrm{Ge}}$ and $M_2=M_{\mathrm{Si}}$.

orders of magnitude smaller than the right peak and consequently contribute nothing to the scattering rates. For this template case ($M_1=M_2=M_t$), the SL is equivalent to a bulk lattice with diamond structure and so the scattering strength of the mini-umklapp processes must vanish in order that the bulk thermal conductivity, $\kappa_t^{(i)}$, is recovered. This is observed in Fig. 2. Increasing the mass ratio from 1 to 1.001, causes the mini-umklapp peak to shift well to the right as these events now begin to contribute to the scattering rates. Further increase of the mass ratio to 1.1 produces the single strong right peak (dotted line in Fig. 2). The absolute number of scattering events that contribute to $\kappa_{\mathrm{SL}}^{(i)}$ is now significantly larger than in the $M_1/M_2=1$ case. However, there is only a very small decrease in $\kappa_{\mathrm{SL}}^{(i)}$ because of the overall decreased magnitudes of $|\Phi|^2$, which manifest themselves as a shift to the left of the contributing peak. As the SL period is increased, the proportion of the total scattering events that are mini-umklapp processes increases rapidly. However the behavior remains, as discussed above.

As the mass ratio is increased further from 1.1 to 2.58 (open squares), the number of scattering events is strongly suppressed while the peak location is only slightly reduced. This suppression reflects the decreased three-phonon phase space for the SL with increasing M_1/M_2, which, as discussed above, acts to raise $\kappa_{\mathrm{SL}}^{(i)}$.

In a previous calculation,[15] we investigated the behavior of $\kappa_{\mathrm{SL}}^{(i)}/\kappa_t^{(i)}$ using a Keating model for the phonon dispersions and anharmonic forces.[16] This model includes only central and bond-bending interactions between nearest-neighbor ions. The qualitative behavior obtained was similar to that discussed above. However, to assess the importance of accurately representing the phonon dispersions, we now compare directly $\kappa_{\mathrm{SL}}^{(i)}/\kappa_t^{(i)}$ obtained from the ABC model and the Keating model. Figure 3 shows the calculated phonon dispersions

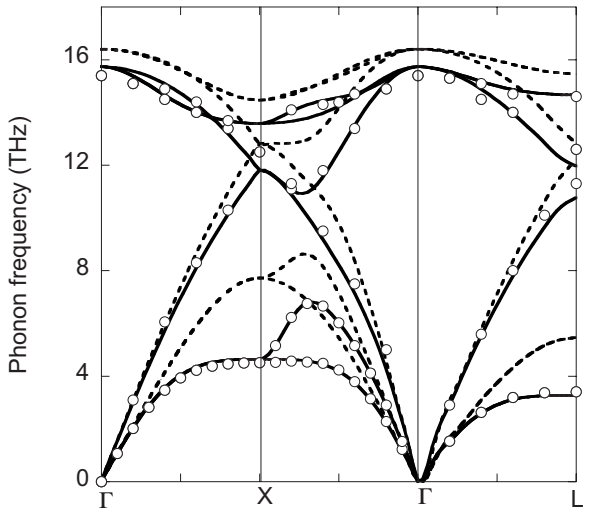

FIG. 3. Si phonon dispersion. Dashed lines: Keating model. Solid lines: ABC model. Open circles: experiment (Ref. 31).

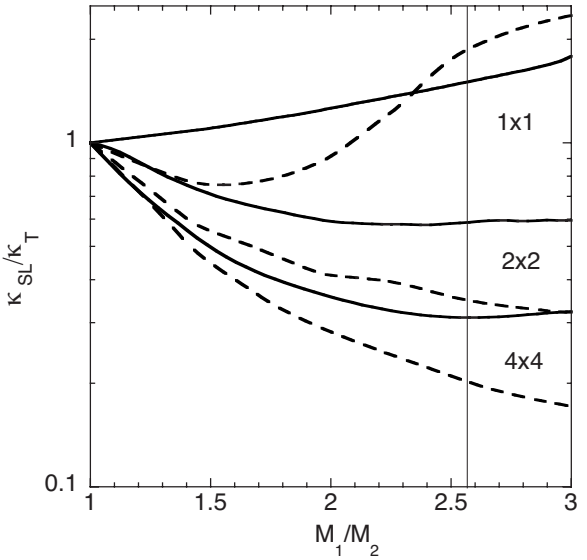

FIG. 4. $\kappa_{\mathrm{SL}}^{(i)}$ for 1×1, 2×2, and 4×4 Si/Ge-based SLs as a function of the mass ratio of constituent atoms, M_1/M_2. The dashed lines are for the Keating model while the solid lines are for the ABC model. The thin vertical line indicates the Ge/Si mass ratio.

for the two models for bulk Si compared with the experimental data.[30] It is evident that the TA branches and the optic branches are represented more accurately using the ABC model. In particular, the Keating model significantly overestimates the TA phonon frequencies for large wave vectors.

As noted above, increasing the mass ratio for the SL flattens the acoustic phonon dispersions, lowering the average group velocity. Since the Keating model has less dispersive acoustic phonon branches, increasing M_1/M_2 produces an unrealistically strong reduction in $\kappa_{\mathrm{SL}}^{(i)}$. In contrast, for the ABC model, the bulk TA branches are already flat over a significant fraction of the Brillouin zone. The effect on TA branch flattening from increasing M_1/M_2 is therefore less pronounced, leading to higher overall values of $\kappa_{\mathrm{SL}}^{(i)}/\kappa_t^{(i)}$ for the ABC model compared to those obtained from the Keating model. This behavior is illustrated in Fig. 4.

For real SL structures the lattice thermal conductivity, κ_{SL}, is determined primarily by a combination of the part due to intrinsic (three-phonon) scattering, $\kappa_{\mathrm{SL}}^{(i)}$, as described above, and by the part due to extrinsic phonon scattering from the SL interfaces, $\kappa_{\mathrm{SL}}^{(e)}$. Direct calculations of $\kappa_{\mathrm{SL}}^{(e)}$ are typically hindered by lack of information about the sample-dependent interface quality. The accurate calculations presented here allow us to investigate the relative strength of $\kappa_{\mathrm{SL}}^{(i)}$ and $\kappa_{\mathrm{SL}}^{(e)}$. It is reasonable to expect that for short-period SLs, the interface scattering will be quite strong as monolayer fluctuations represent a significant fraction of the SL period. Recently calculations of $\kappa_{\mathrm{SL}}^{(i)}$ have been performed for GaAs/AlAs SLs within the CRTA using a rigid-ion model,[31] which accurately represents the phonon dispersions. That work found roughly a threefold reduction in the room temperature $\kappa_{\mathrm{SL}}^{(i)}$ of 3×3 SLs compared to bulk GaAs and it concluded that this number represented an upper bound if the phonon lifetime is reduced by the mini-umklapp scattering, as suggested by Ren and Dow.[19] The measured room-temperature lattice thermal conductivity, κ_{SL}, for 3×3 GaAs/AlAs SLs was found to be reduced by a factor of about seven compared to bulk GaAs.[4] Assuming that Matheissen's rule holds: $1/\kappa_{\mathrm{SL}}\approx1/\kappa_{\mathrm{SL}}^{(i)}+1/\kappa_{\mathrm{SL}}^{(e)}$, the CRTA results from Ref. 31 suggest that the intrinsic and extrinsic contributions are about the same. This result is surprising because, as pointed out above, we expect the extrinsic contribution to dominate the behavior of κ_{SL}.

We have calculated $\kappa_{\mathrm{SL}}^{(i)}$ for $N\times N$ GaAs/AlAs SLs (Ref. 32) using the approach presented here. We find that the phonon lifetimes are in fact *increased* compared to bulk GaAs. As for the Si/Ge case, this occurs because the enhancement resulting from the reduced three-phonon phase space outweighs the decrease from the added mini-umklapp scattering. Our calculated room temperature $\kappa_{\mathrm{SL}}^{(i)}$ for 1×1, 2×2, and 3×3 SLs are: 36.8, 27.4, and 26.6 W/m-K, respectively. Thus, for the 3×3 SL we find a reduction of 1.7, about half of that found in Ref. 32. From Matheissen's rule, this gives a reduction due to extrinsic phonon scattering that is roughly three times larger than that due to intrinsic scattering, a result that is qualitatively consistent with our expectations.

Figure 5 highlights the contrast between the results from our full calculation and the CRTA results. The dotted, dashed, and solid lines in Fig. 5 show our calculated $\kappa_{\mathrm{SL}}^{(i)}$ for 1×1, 2×2, and 3×3 SLs, respectively, as a function of temperature. The CRTA results at 100, 200, and 300 K for 2×2 and 3×3 SLs (Ref. 31) are labeled by the solid triangles and open squares. Also shown are the measured lattice thermal conductivities of bulk GaAs (Ref. 27) (solid circles), and the 1×1 (plusses), 2×2 (crosses), and 3×3 (open triangles) GaAs/AlAs SLs.[4] There are several points to notice. First, the temperature dependence of the calculated SL thermal conductivities is quite similar to that for bulk GaAs. This is true because the GaAs samples are high quality so that three-phonon scattering is dominant. Conversely, the GaAs/AlAs SLs show a significantly different dependence on the temperature.

Second, the calculated $\kappa_{\mathrm{SL}}^{(i)}$ values obtained from our approach show only a modest reduction compared to those of bulk GaAs by factors of 1.2 for 1×1 SLs, and 1.7 for 2

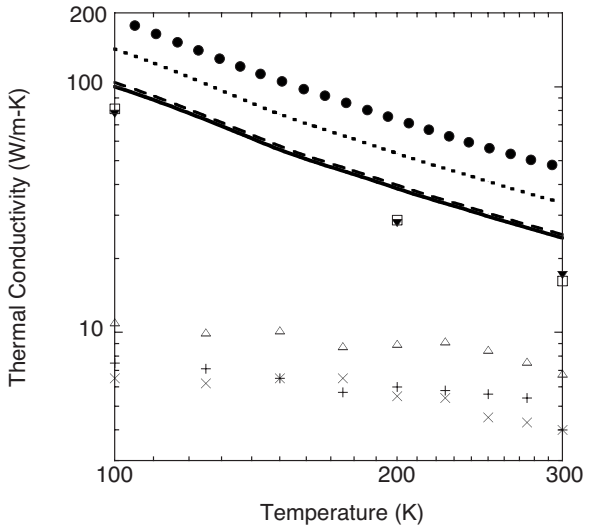

FIG. 5. $\kappa_{\mathrm{SL}}^{(i)}$ for 1×1 (dotted line), 2×2 (dashed line), and 3×3 (solid line) GaAs/AlAs SLs as a function of temperature compared to the CRTA results for 2×2 (solid triangles) and 3×3 (open squares) SLs, and to measured lattice thermal conductivities of bulk GaAs (solid circles), as well as measurements for 1×1 (plusses), 2×2 (crosses), and 3×3 (open triangles) GaAs/AlAs SLs (Ref. 4).

$\times2$ and 3×3 SLs over the full temperature range. On the other hand, the experimental values from Ref. 4 are significantly lower than the bulk GaAs values. This fact combined with the different measured temperature dependence suggests that the dominant scattering mechanism in these SLs is extrinsic and provided by interface scattering of phonons. This is consistent with the rough interfaces expected for short-period SLs and with the results of molecular-dynamics simulations.[33]

In contrast with the above finding, the CRTA results show that the intrinsic and extrinsic scattering mechanisms are approximately of equal importance at room temperature, as discussed above. This stark difference highlights the importance of using the rigorous approach presented in our manuscript in obtaining quantitatively and qualitatively significant results.

V. SUMMARY AND CONCLUSIONS

Using an accurate description of phonon dispersions and an empirical model for anharmonic scattering, the intrinsic lattice thermal conductivity, $\kappa_{\mathrm{SL}}^{(i)}$, of Si/Ge-based and GaAs/AlAs SLs has been calculated in an exact solution of the Boltzmann transport equation for phonons. Decreases in $\kappa_{\mathrm{SL}}^{(i)}$ occurred with increasing mass ratio of the constituent atoms and increasing SL periods. However, for both SL systems considered, the decreases in $\kappa_{\mathrm{SL}}^{(i)}$ are not as large as observed using constant relaxation-time approximations and simple phonon-dispersion models. This is explained by the decrease in the phase space for three-phonon scattering and the inclusion of accurate descriptions of the heat carrying acoustic branches. The approach presented here has been used to indirectly extract the extrinsic contribution, $\kappa_{\mathrm{SL}}^{(e)}$, to the thermal conductivity of GaAs/AlAs SLs. A more significant role for interface scattering is found than predicted from a constant relaxation-time approach[31] in accordance with physical expectations.

We note finally that for a given material system and superlattice structure, the extrinsic contribution to the thermal conductivity of SLs can vary widely from sample to sample while the intrinsic contribution is fixed. The accurate approach developed here can then provide a useful baseline from which the significance of phonon interface scattering and hence SL quality can be evaluated. With continuing improvements in materials fabrication technology, SL interface quality will likely improve, making it even more important to have an accurate theoretical approach to calculate $\kappa_{\mathrm{SL}}^{(i)}$.

ACKNOWLEDGMENTS

This research was supported in part by the National Science Foundation under Grant No. 0651381. Acknowledgment is also made to the Donors of the American Chemical Society Petroleum Research Fund for partial support of this research.

APPENDIX: THE ABCM FOR [001] Si/Ge AND GaAs/AlAs SLs

For direct central potential interactions between two basis particles, the harmonic force constants are

$$\Phi_{\alpha\beta}=-\frac{X_\alpha X_\beta}{r_0^2}\left(\phi''-\frac{\phi'}{r_0}\right)-\delta_{\alpha\beta}\frac{\phi'}{r_0}, \tag{A1}$$

where r_0 is the equilibrium distance between the two particles, X_α is the αth component of this distance, and ϕ' and ϕ'' are the first and second derivatives of the central potential evaluated at the equilibrium distance. The ion-bc force constants arising from the bond-bending interaction[16,17] is

$$\Phi_{\alpha\beta}^{(bb)}(\text{ion }\ \kappa,bc\ \ i)=-\frac{\beta_k^{(\kappa)}}{a^2}\sum_{j\neq i}X_{j\alpha}(X_{i\beta}+X_{j\beta}), \tag{A2}$$

where a is the lattice constant and $\beta_k^{(\kappa)}$ is the Keating IFC that measures the strength of the bc-ion-bc bond-bending forces with central ion labeled by $\kappa=1,2$. In the transformed coordinate system of the SL, the ion 1-bc force-constant matrix describing the direct interaction between ion 1 at (0,0,0) and bc 5 at $(h_1/4,0,a/8)$, using Eq. (A1), is obtained as

$$\Phi_{i-bc}(\ell1,\ell5)=-\begin{bmatrix}\alpha_1+\beta_1 & 0 & \sqrt{2}\beta_1\\ 0 & \alpha_1-\beta_1 & 0\\ \sqrt{2}\beta_1 & 0 & \alpha_1\end{bmatrix},$$

$$\alpha_1=\tfrac{1}{3}\phi_{i-bc}''^{(1)}+\tfrac{2}{3}\phi_{i-bc}'^{(1)}/r_0+\tfrac{1}{2}\beta_k^{(1)},$$

$$\beta_1=\tfrac{1}{3}\phi_{i-bc}''^{(1)}-\tfrac{1}{3}\phi_{i-bc}^{(1)}/r_0-\tfrac{1}{2}\beta_k^{(1)}. \tag{A3}$$

Force constant matrices for ion 1, interacting with its other three nearest-neighbor bc, are obtained in a similar manner. The form of the ion-ion matrices is the same with force constants α' and β' replacing α_1 and β_1. For the bond-bending

interaction with central ion $\kappa=1$, the force constants for bc i and bc j are[16,17]

$$\Phi_{\alpha\beta}^{(bb)}(i,j) = -\frac{\beta_k^{(\kappa)}}{a^2} X_{j\alpha} X_{i\beta}. \tag{A4}$$

The IFC matrix between bc 5 and bc 6 [at $(-h_1/4, 0, a/8)$] is

$$\Phi_{bc-bc}(\ell 5, \ell 6) = -\begin{bmatrix} \mu_1 + \nu_1 & 0 & \sqrt{2}\delta_1 \\ 0 & \mu_1 - \nu_1 & 0 \\ -\sqrt{2}\delta_1 & 0 & \lambda_1 \end{bmatrix},$$

$$\mu_1 = \nu_1 = \beta_k^{(1)}/4 + \psi_1''/2, \quad \delta_1 = -\lambda_1 = \beta_k^{(1)}/4,$$

$$\psi_1'' = -\psi_2'' = (\beta_k^{(2)} - \beta_k^{(1)})/8. \tag{A5}$$

In Si/Ge-based SLs, the atoms have equal charge so $\alpha_1=\alpha_2 \equiv \alpha$, etc. Also, we take the geometric average of the harmonic IFCs defined for each bulk material: $\alpha=\sqrt{\alpha_{\mathrm{Si}}\alpha_{\mathrm{Ge}}}$. For the GaAs/AlAs SLs, we take separately the geometric average of the cation IFCs and anion IFCs: $\alpha_1=\sqrt{\alpha_{\mathrm{Ga}}\alpha_{\mathrm{Al}}}$, $\alpha_2=\alpha_{\mathrm{As}}$, etc.

For evaluation of Ewald transformations required to determine the Coulomb force constants, sums over direct and reciprocal-lattice shells are calculated where the number of shells taken must be sufficient to achieve convergent results. We find that the number of required shells increases with SL period. For example, for a 2×2 Si/Ge SL, seven shells are sufficient while for an 8×8 superlattice, 14 shells are required.

The nearest-neighbor anharmonic central ion-ion force constants are obtained from[34]

$$\Phi_{\alpha\beta\gamma} = -\left[\frac{X_\alpha X_\beta X_\gamma}{r_0^3}\left(\phi''' - 3\frac{\phi''}{r_0} + 3\frac{\phi'}{r_0^2}\right) + \frac{1}{r_0^2}\left(\phi'' - \frac{\phi'}{r_0}\right)(X_\alpha\delta_{\beta\gamma} + X_\beta\delta_{\alpha\gamma} + X_\gamma\delta_{\alpha\beta})\right]. \tag{A6}$$

Here, ϕ' and ϕ'' are known from the ABC model while ϕ''' is chosen so that the calculated room-temperature lattice thermal conductivity of each bulk material considered matches the corresponding measured values.

[1] D. G. Cahill, W. K. Ford, K. E. Goodson, G. D. Mahan, A. Majumdar, H. J. Maris, R. Merlin, and S. R. Phillpot, J. Appl. Phys. **93**, 793 (2003).
[2] S.-M. Lee, D. G. Cahill, and R. Venkatasubramanian, Appl. Phys. Lett. **70**, 2957 (1997).
[3] W. S. Capinski and H. J. Maris, Physica B (Amsterdam) **219&220**, 699 (1996).
[4] W. S. Capinski, H. J. Maris, T. Ruf, M. Cardona, K. Ploog, and D. S. Katzer, Phys. Rev. B **59**, 8105 (1999).
[5] R. Venkatasubramanian and T. Colpitts, in *Thermoelectric Materials—New Directions and Approaches*, edited by T. M. Tritt, M. G. Kanatzidis, H. B. Lyons, Jr., and G. D. Mahan, MRS Symposia Proceedings No. 478 (Materials Research Society, Pittsburgh, 1997), p. 73.
[6] Deyu Li, Yiying Wu, R. Fan, Peidong Yang, and Arun Majumdar, Appl. Phys. Lett. **83**, 3186 (2003).
[7] Deyu Li, Yiying Wu, Philip Kim, Li Shi, Peidong Yang, and Arun Majumdar, Appl. Phys. Lett. **83**, 2934 (2003).
[8] G. D. Mahan, B. Sales, and J. Sharp, Phys. Today **50**(3), 42 (1997).
[9] F. Di Salvo, Science **285**, 703 (1999).
[10] G. Chen, Phys. Rev. B **57**, 14958 (1998).
[11] R. E. Peierls, *Quantum Theory of Solids* (Oxford University Press, Oxford, 1955).
[12] J. M. Ziman, *Electrons and Phonons* (Oxford University Press, London, 1960).
[13] P. Hyldgaard and G. D. Mahan, Phys. Rev. B **56**, 10754 (1997).
[14] Shin-ichiro Tamura, Yukihiro Tanaka, and Humphery J. Maris, Phys. Rev. B **60**, 2627 (1999).
[15] D. A. Broido and T. L. Reinecke, Phys. Rev. B **70**, 081310(R) (2004).
[16] P. N. Keating, Phys. Rev. **145**, 637 (1966); **149**, 674 (1966).
[17] W. Weber, Phys. Rev. B **15**, 4789 (1977).
[18] K. C. Rustagi and W. Weber, Solid State Commun. **18**, 673 (1976).
[19] S. Y. Ren and J. D. Dow, Phys. Rev. B **25**, 3750 (1982).
[20] M. Omini and A. Sparavigna, Phys. Rev. B **53**, 9064 (1996).
[21] M. Omini and A. Sparavigna, Nuovo Cimento D **19**, 1537 (1997).
[22] D. A. Broido, A. Ward, and N. Mingo, Phys. Rev. B **72**, 014308 (2005).
[23] D. A. Broido, M. Malorny, G. Birner, Natalio Mingo, and D. A. Stewart, Appl. Phys. Lett. **91**, 231922 (2007).
[24] A. A. Maradudin, E. W. Motroll, G. H. Weiss, and I. P. Ipatova, *Solid State Physics* (Academic, New York, 1971), Suppl. 3.
[25] V. Inyushkin, A. N. Taldenkov, A. M. Cibin, A. V. Gusev, and H.-J. Pohl, Phys. Status Solidi C **1**, 2995 (2004); R. K. Kremer, K. Graf, M. Cardona, G. G. Devyatykh, A. V. Gusev, A. M. Gibin, A. V. Inyushkin, A. N. Taldenkov, and H.-J. Pohl, Solid State Commun. **131**, 499 (2004).
[26] V. I. Ozhogin, A. V. Inyushkin, A. N. Taldenkov, A. V. Tikhomirov, and G. E. Popov, JETP Lett. **63**, 490 (1996).
[27] A. V. Inyushkin, A. N. Taldenkov, A. Yu Yakubovsky, A. V. Markov, L. Moreno-Garsia, and B. N. Sharonov, Semicond. Sci. Technol. **18**, 685 (2003).
[28] E. F. Steigmeier and I. Kudman, Phys. Rev. **141**, 767 (1966).
[29] R. Venkatasubramanian, Phys. Rev. B **61**, 3091 (2000).
[30] G. Nilsson and G. Nelin, Phys. Rev. B **6**, 3777 (1972).
[31] W. E. Bies, R. J. Radtke, and H. Ehrenreich, J. Appl. Phys. **88**, 1498 (2000).
[32] In our notation, the *NxN* GaAs/AlAs superlattice has $4N$ atoms per superlattice unit cell, in contrast with the Si/Ge superlattice, which has $2N$ atoms per unit cell.
[33] B. C. Daly, H. J. Maris, K. I. Imamura, and S. Tamura, Phys. Rev. B **66**, 024301 (2002).
[34] A. A. Maradudin, in *Dynamical Properties of Solids*, edited by G. K. Horton and A. A. Maradudin (North-Holland, Amsterdam, 1974), pp. 3–82.